processes

MDPI

Article

Response Surface Methodology—Central Composite Design Optimization Sugarcane Bagasse Activated Carbon under Varying Microwave-Assisted Pyrolysis Conditions

Xuexue Chen [1,†], Yunji Pei [1,†], Xinran Wang [1], Wenlin Zhou [2] and Li Jiang [1,*]

[1] School of Resources and Environmental Engineering, Jiangsu University of Technology, Changzhou 213001, China; 15185322732@163.com (X.C.); 13685249983@163.com (Y.P.); 15615685812@163.com (X.W.)
[2] Laboratory and Equipment Management Center, Jiangsu University of Technology, Changzhou 213001, China; wlzhou@jsut.edu.cn
* Correspondence: jl@jsut.edu.cn
† These authors contributed equally to this work.

Abstract: Sugarcane bagasse (SB) is a widely available agro-industrial waste residue in China that has the potential to be converted into a cost-effective and renewable adsorbent. In this study, activated carbon (AC) was prepared from SB by microwave vacuum pyrolysis using H_3PO_4 as the activator. To enhance the sorption selectivity and yield, the pyrolysis process of SB-activated carbon (SBAC) should be well-designed. Central composite design was employed as an optimized experiment design, and response surface methodology was used to optimize the process parameters for maximized SBAC yield and its iodine number. The results showed that the optimized parameters obtained for the SBAC are 2.47 for the impregnation ratio (IR), 479.07 W for microwave power (MP), 23.86 mm for biomass bed depth, and 12.96 min for irradiation time, with responses of 868.7 mg/g iodine number and 43.88% yield. The anticipated outcomes were substantiated, revealing a marginal 5.4% variance in yield and a mere 1.9% discrepancy in iodine number from the forecasted values. The synthesized adsorbents underwent comprehensive characterization through instrumental methodologies, including FT-IR, BET, and SEM. The SBAC produced by the pyrolysis method contained a regular and homogeneous porous structure with a specific surface area of up to 1697.37 m^2/g and a total 1.20 cm^3/g volume, which has favorable adsorption of toxic and harmful substances in the environment.

Keywords: sugarcane bagasse; activated carbon; response surface methodology; optimization; microwave pyrolysis

Citation: Chen, X.; Pei, Y.; Wang, X.; Zhou, W.; Jiang, L. Response Surface Methodology—Central Composite Design Optimization Sugarcane Bagasse Activated Carbon under Varying Microwave-Assisted Pyrolysis Conditions. *Processes* **2024**, *12*, 497. https://doi.org/10.3390/pr12030497

Academic Editors: Adam Smoliński and Nikolay Yu. Peskov

Received: 22 January 2024
Revised: 9 February 2024
Accepted: 17 February 2024
Published: 28 February 2024

1. Introduction

The recovery and recycling of abundant natural resources, such as agricultural residues, to produce value-added products is an imminent issue currently facing the world. Globally, 1.3 million tons of agricultural biomass are generated annually [1], examples of which include agricultural waste, sludge, plant hulls, animal waste, and a range of other biomass materials [2,3]. Unlike the negative effects caused by inappropriate disposal of agricultural waste, recycling agricultural waste not only contributes to environmental protection and economic development but also makes agricultural waste a promising alternative to carbon-based materials. Ideally, the next generation of carbon-based materials needs to be produced using renewable resources via a simple, cost-effective, and environmentally friendly method [2,4].

China, the world's fifth-largest sugar producer, produced 11.788 million tons of sugar in 2022 (NDRC, http://www.ndrc.gov.cn/ (accessed on 19 January 2023)). Sugarcane is one of China's most important sugar crops, and sugarcane production reached 106.664 million tons in 2021, accounting for 93.12% of sugar crops (NBSC, http://www.stats.gov.cn/

(accessed on 14 December 2021)). Sugarcane bagasse (SB) is an essential inedible by-product of sugarcane production which is usually produced by extracting sugar juice from sugarcane, and accounts for about 30–50% of the mass of sugarcane [5–7]. In 2021, it was estimated that SB production would reach as much as 5,333,200 tons. SB is primarily used for the production of bioethanol [8]. Liu [9] studied the production of cellulosic ethanol with a maximum yield of up to 0.70 g/(L/h) from SB. Wang [10] pretreated the SB under low-temperature conditions with sodium hydroxide, and the ethanol yield reached 67.5%. Dionísio [11] found that pretreatment of bagasse with diluted sulfuric acid yields up to 86.11% ethanol. Although the main research trend of SB is to convert it into bioethanol, industrial application is difficult due to its high cost and long conversion time [12]. Thermal conversion technology is comparatively a better choice because the process recycles and utilizes all the by-products, has a short reaction time, and offers ease of operation and regulation [13]. Pyrolysis is a thermal decomposition technology for the conversion of carbonaceous materials into energy and compounds with added value (biochar, pyrolysis oil, or gas mixtures) [14].

Conventional pyrolysis and microwave pyrolysis are commonly categorized [15] as the main conversion methods. The primary difference between them is the method of heating; the microwave technique encompasses volumetric heating, while traditional pyrolysis relies on either conduction or convection heating [16,17]. Conventional pyrolysis normally operates in batch, semi-batch, or continuous reactors with low heating efficiency (10 °C/min) [18,19]. However, microwave-assisted pyrolysis proves to be more effective in heating because microwave radiation heats the entire substance uniformly, instead of from the sample's surface, as in conventional methods [19]. Thus, microwave heating is advantageous in providing fast heating (43 °C/min) and shorter reaction times (20–40 min) [20]. The advantages of microwave pyrolysis have attracted many researchers to use microwave pyrolysis to optimize different organic raw materials, such as xylan and microcrystalline cellulose [21], baby diapers [20], amino acids [22], corn cobs [23], and bagasse [15]. These studies are good proof that microwave pyrolysis treatment of biomass is not only time-saving but also results in better product quality.

Microwave and conventional pyrolysis of biomass is usually carried out under inert gases such as N_2 to maintain an oxygen-free environment for pyrolysis to take place [24,25]. Even though previous studies have demonstrated the benefits of microwave pyrolysis for biomass utilization, the continuous use and consumption of N_2 have contributed to higher operating costs, limiting scale-up and industrial applications [26]. The vacuum pyrolysis environment of microwave vacuum pyrolysis (MVP) replaces the commonly used N_2 environment, reducing the use and consumption of N_2, and the negative pressure conditions aid in accelerating the thermal cracking reaction and aid in the discharge of the pyrolysis volatiles, producing AC with higher yields and cleaner pores [27]. Liew [28] used MVP to produce palm kernel shell-derived char, which resulted in up to 89 wt% yields of AC with a high surface area (750 m^2/g) and pore volume (up to 0.37 cm^3/g). The application of corn cobs as a feedstock to synthesize corn cob activated carbon (CCAC) via MVP was investigated by He [23], whose research showed the specific surface area and pore volume were 995.09 m^2/g and 0.708 cm^3/g, respectively. Meanwhile, performance tests showed that the iodine number and yield reached 933.38 mg/g and 37.57%, respectively. Therefore, microwave heating has been selected as the heat source to heat and pyrolyze SB under an oxygen-starved ambience created by a vacuum pump. However, as with most production processes, the production of high-quality AC involves balancing a number of parameters to obtain the desired output characteristics [23]. Usually, this balancing becomes complicated because more than one characteristic must be considered. We tend to optimize parameters in this paper.

Several studies regarding SB pyrolysis have been reported. The composites obtained by L. Rodier by mixing SB biochar with cement are more flexible and favorable for the construction of houses in seismic areas [29]. Guo [30] obtained high-quality AC with a high specific surface area (1149 m^2/g), large pore volume (1.73 cm^3/g), and an extraordinarily

high CO_2 uptake of 4.28 mmol CO_2/g by treating bagasse modified with sodium hydroxide. Torgbo's [31] study shows that SB can be used as a precursor for the production of value-added products such as cellulose nanocrystals, cellulose nanofibers, and microcrystalline cellulose. However, no information is available in the previous studies that present how bed depth affects SBAC yield and absorption characteristics. Salema [32] found that penetration depth plays a vital role in microwave energy absorption by a sample. It means that SB bed depth is equal to other parameters, such as microwave power (MP), microwave irradiation time, etc., during the process of SBAC production. To the authors' knowledge, research regarding this topic is insufficient. The effects of the combination of four process parameters (impregnation ratio (IR), irradiation time, MP, and biomass bed depth) on output, optimizing biomass waste carbonization factors by facile and sustainable routes, would benefit industries seeking to produce SBAC via a low-cost and eco-friendly solution.

This research aims to optimize the process parameters from SB using H_3PO_4 to produce high-adsorption-efficiency SBAC. Response surface methodology (RSM)–central composite design (CCD) was used to study simultaneously the effects of four preparation variables (IR, irradiation time, MP, and biomass bed depth) on the iodine number and yield as response.

2. Materials and Methods

2.1. Experimental Materials

The raw SB (Hangzhou, China) purchased from Taobao.com (https://tb.alicdn.com/) was used as feedstock material in this study. The original particle size of feedstocks ranges from 10 mm to 15 mm.

2.2. Preparation of SBAC

A custom-made microwave pyrolysis system was used in this study (Nanjing, China). A 2.45 GHz microwave oven was modified by combining with a vacuum pump to perform microwave vacuum pyrolysis experiments. An 1800 W vacuum pump was used to withdraw the air from inside the microwave oven continuously to maintain vacuum conditions at −0.04 to −0.06 MPa. The pressure inside the microwave reactor was measured using a pressure gauge. A pyrolysis reactor (quartz material, 2.48 L) was utilized while the sample's temperature was monitored by a K-type thermocouple.

The raw SB underwent washing twice with distilled water to eliminate dust particles before undergoing a 12 h drying process. Subsequently, the dried SB was subjected to crushing at 105 °C to eliminate residual water content. The resulting granules were sieved through a 100-mesh filter to achieve the desired particle size. Following this, the SB particles underwent impregnation with a specified concentration (14.7 mol/L) of H_3PO_4 (Jiangsu, China) for a duration of 12 h.

The desiccated pellets were subsequently subjected to microwave vacuum pyrolysis equipment for the synthesis of SBAC. The production of SBAC involved varying parameters such as IR, MP, biomass bed depth, and irradiation time. Following the heating process, the system underwent a cooling process to reach room temperature. Subsequently, the acquired samples were thoroughly washed with a solution containing 10% HCl (Shanghai, China) and distilled water until the pH of the washing solution reached a neutral range between 6 and 7. Following the washing procedure, the samples were dried at a temperature of 105 °C and ultimately sieved to achieve a size of 200 mesh before being stored in a desiccator (Shanghai, China). The SBAC preparation process is shown in Figure 1.

IR is defined as the ratio of the mass of the chemical agent to the precursor; it is estimated by Equation (1).

$$\mathrm{IR} = \frac{\text{weight of } H_3PO_4}{\text{weight of sugarcane bagasse}} \quad (1)$$

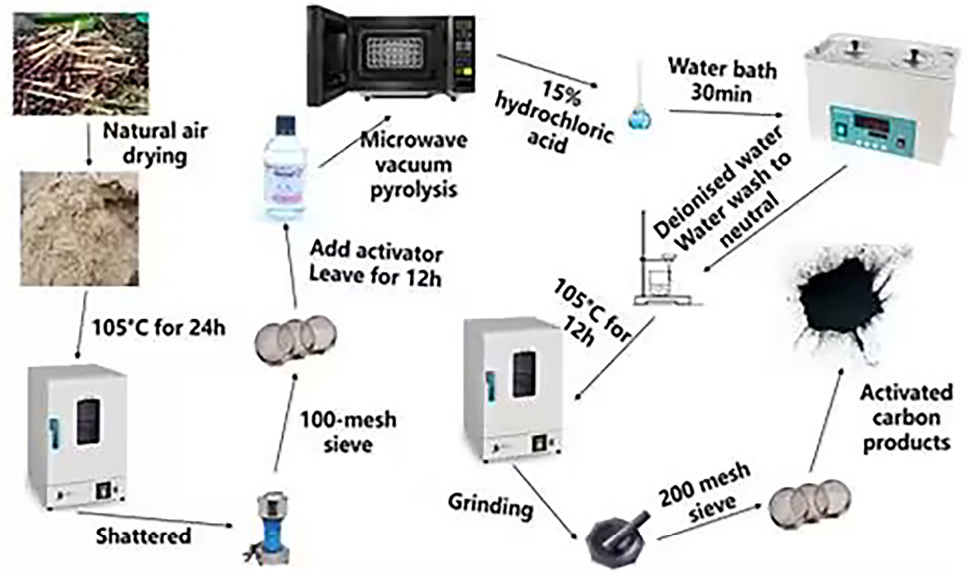

Figure 1. SBAC preparation process.

2.3. Design of Experiments Using RSM

Statistical design of experiments has been widely used in medicine [33], food [34], chemistry [35], and environmental engineering [36] as an effective way to improve experimental work. Among common statistical methodologies, RSM is considered an effective technique capable of assessing the interactions on the prediction variables and their responses, which identifies the combination of factors that produces an optimal response with the advantages of fewer experiments and higher accuracy [37]. Preliminary experiments were conducted by prior arrangement for determining the feasibility; the preliminary experimental data are shown in Section 3.1. Based on the preliminary results, the parameter ranges for IR, MP, biomass bed depth, and irradiation time were set from 1 to 3, 200 to 600 W, 10 to 30 mm, and 10 to 14 min, respectively; the maximum and minimum values that have been keyed into the model are also provided in Table 1. Iodine number (Y_1) and yield (Y_2) were designated as responses.

Table 1. Coded and actual levels for independent factors used in the experimental design.

Factors	Units	Code	Coded Variable Levels				
			−a	−1	0	+1	+a
IR		A	1	1.5	2	2.5	3
MP	W	B	200	300	400	500	600
biomass bed depth	mm	C	10	15	20	25	30
Microwave irradiation time	min	D	10	11	12	13	14

2.4. Determination of Iodine Number and AC Yield

The iodine number is a widely used technique employed to determine the adsorption capacity of AC. The iodine number indicates the porosity of AC and it is defined as the amount of iodine number by 1 g of carbon at the mg level. In this study, a Chinese official standard (https://openstd.samr.gov.cn/ (accessed on 3 July 2015)) was used to test adsorption capacity of AC.

Biochar yield is a pivotal metric for evaluating the thermal convertibility properties of AC, reflecting the efficiency and stability of biochar production, and refers to the ratio of the mass of biochar product obtained to the mass of the feedstock, thereby describing

how much of the original mass remains in the solid residue of pyrolysis. The calculation formula is as follows:

$$\text{Yield} = \frac{\text{weight of actived carbon}}{\text{weight of sugarcane bagasse}} \quad (2)$$

2.5. Characterization of SBAC

Characterizations of biomass feedstocks and biochar produced under the optimal parameters were analyzed. FT-IR spectra of raw materials and samples were recorded in the range of 400–4000 cm^{-1} at room temperature using a Nicolet Nexus 470 FTIR aerator. Brunauer–Emmett–Teller (BET) and total porosity were determined using a Mack ASAP2460 fully automated specific surface and porosity analyzer with a nitrogen molecular cross-sectional area of 0.162 nm^2 as the basis for calculation. A scanning electron microscope (SEM) was utilized to examine the microscopic morphology present on the surface of SBAC samples.

3. Results and Discussion

3.1. Effect of Process Parameters on SBAC Yield and Iodine Number

3.1.1. Effect of IR

The IR is a critical factor for the development of pores in adsorbent materials. At MP of 400 W, biomass bed depth of 20 mm, and microwave irradiation time of 11 min, the IR was varied from (1:1) to (1:3) to explore the effects of iodine number and yield.

As shown in Figure 2A, there are differences in the iodine number of SBAC with the change in IR. The IR values of the SBAC prepared by H_3PO_4 activation were increased with increasing IR from (1:1) to (1:2.5) and decreased with increasing IR from (1:2.5) to (1:3). The highest iodine number achieved was 846.69 mg/g when the IR was 2.5. Augmenting the H_3PO_4 content results in a more thorough activation process, fostering the development of a robust porous structure and consequently enhancing adsorption efficiency. However, an excessive quantity of H_3PO_4 can lead to the erosion of the carbon framework, resulting in a thinning of the inter-pore space or even incineration, thereby diminishing the pore number of the adsorbent and reducing its adsorption efficiency [38]. AC yields ranged from 44.93% to 47.58%.

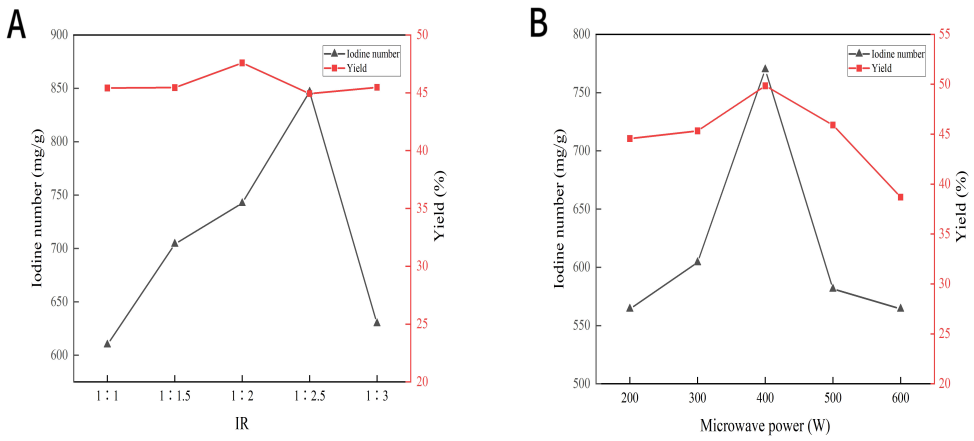

Figure 2. *Cont.*

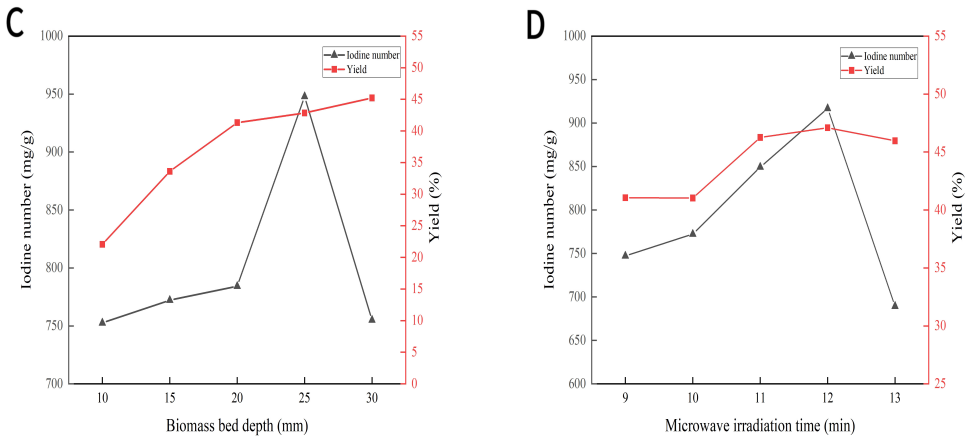

Figure 2. Effect of operating factors on AC yield and iodine number of (**A**) IR, (**B**) MP, (**C**) biomass bed depth, and (**D**) microwave irradiation time.

3.1.2. Effect of MP

SBAC was synthesized under microwave radiation with MP being 200, 300, 400, 500, and 600 W, while the IR was (1:2), the microwave irradiation time was 11 min, and the biomass bed depth was 20 mm, to examine the effects of MP on iodine number and yield.

Figure 2B graphically represents SBAC yield and its iodine number as a function of MP. It can be seen that both the iodine number and SBAC yield initially increase with the rise in MP but as the MP is further increased, the iodine number and yield of SBAC are diminished. When the MP was 200 W, the iodine number was only 564.32 mg/g, indicating poor pore development. At 400 W MP, the iodine number reached a maximum value of 769.85 mg/g, indicating that higher MP provides more effective carbon to generate pores [39], and the decrease in yield after 400 W is due to a series of de-oxidation and de-carboxylation reactions occurring in the pyrolysis process [40]. The increase in MP to 600 W revealed a decrease in yield from 49.85% (at 400 W) to 38.69%, which could be attributed to the progressive expansion of the AC micropores to form mesopores and macropores, resulting in a gradual decrease in the iodine number with the increase in MP.

3.1.3. Effect of Biomass Bed Depth

Figure 2C is a plot of SBAC yield and its iodine number as a function of biomass. The IR (1:2), MP (400 W), and microwave irradiation time (11 min) were set and the biomass bed depth was varied from 10 to 30 mm, to examine the effects of biomass bed depth on iodine number and yield.

The iodine number of SBAC increased gradually from the lowest value of 752.30 mg/g by increasing the height of the biomass bed from 10 mm to 30 mm, and the iodine number reached a maximum of 947.92 mg/g when the height of the biomass bed reached 25 mm and then decreased. SBAC yield was increased by increasing the biomass bed depth within the investigated conditions; increasing the biomass bed depth from 10 to 30 mm increased the SBAC yield from 22.06% to 45.21%. It has been established that the loading biomass bed depth affects microwave energy absorption. This means that there is an optimal biomass bed depth at which the maximum microwave energy is absorbed, thereby reaching the optimal temperature profile [41].

3.1.4. Effect of Irradiation Time

Figure 2D shows the variation in SBAC yield and its iodine number with microwave irradiation time. The iodine number and yield of SBAC increased from 9 min to 12 min (824.15 mg/g to 916.77 mg/g, 41.06% to 74.09%) as the carbon in the feedstock was activated to produce more pores and release volatiles. The sharp decrease in iodine number after 12 min indicates that the easily decomposed substances have been reacted completely, while the increase in ash produced by the pyrolysis of SB leads to a decrease in the iodine

number [42,43]. A medium residence time is essential to ensure adequate carbonization and activation of the raw material.

3.2. Optimization of Process Parameters

Through the various combinations of parameters, 30 experiments were designed and executed.

3.2.1. Optimization of Process Variables Using CCD

Table 2 shows the SBAC optimization experiment matrix and results. In 30 experimental runs, runs 7, 8, 11, 25, 27, and 30 having the same factor levels, the pure error of the experiments was tested through the repetition of six sets of center point experiments. A smaller pure error indicates a higher degree of experimental precision and a higher degree of confidence in the experimental data.

Table 2. SBAC optimization experiment matrix and results.

Run No	A	B	C	D	Iodine Number Y_1/mg/g	Yield Y_2 (%)
	IR	MP/W	Height of Biomass Bed/mm	Microwave Irradiation Time/min		
1	2	400	20	10	658.23	36.38
2	2.5	300	15	13	668.11	39
3	1.5	300	15	11	532.46	32.44
4	2.5	500	15	13	720.34	42.31
5	1.5	500	15	11	516.38	35.18
6	2	400	10	12	731.66	35.33
7	2	400	20	12	916.57	46.56
8	2	400	20	12	937.63	48.2
9	1.5	300	15	13	572.91	34.08
10	2	400	20	14	675.02	41.07
11	2	400	20	12	909.3	47.68
12	2.5	500	25	13	696.73	41.75
13	2.5	500	15	11	775.53	42.25
14	1.5	500	25	11	613.62	33.32
15	2	200	20	12	357.77	33.11
16	1.5	300	25	13	534.27	41.4
17	2.5	300	25	13	549.38	39.48
18	3	400	20	12	598.18	41.33
19	2.5	300	15	11	548.56	34.81
20	2.5	500	25	11	679.81	39.39
21	1	400	20	12	477.07	31.8
22	2	600	20	12	689.35	34.47
23	1.5	500	25	13	635.47	36.48
24	1.5	300	25	11	443.83	33.7
25	2	400	20	12	930.36	48.2
26	2.5	300	25	11	438.98	35.83
27	2	400	20	12	881.62	46.06
28	1.5	500	15	13	513.35	32.12
29	2	400	30	12	627.69	38.77
30	2	400	20	12	916.8	47.27

3.2.2. ANOVA and Fitting Quadratic Model

The analysis of variance (ANOVA) generated by RSM is presented in Tables 3 and 4. Quadratic polynomial regression models were formulated to anticipate the SBAC response concerning iodine number and yield. Equations (3) and (4) can be employed to forecast the iodine number and yield of SBAC, respectively. The significance of the models and each process variable were assessed using the *p*-value and F-value of the model. A larger F-value

corresponds to a lower associated "problematic P" value, indicating greater significance of the respective coefficient [44].

Table 3. ANOVA for iodine number of SBAC.

Source	Sum of Squares	df	Mean Square	F-Value	*p*-Value	
Model	736,283.399	14	52,591.671	48.371	<0.0001	Significant
A	38,189.88	1	38,189.888	35.125	<0.0001	
B	97,014.17	1	97,014.179	89.229	<0.0001	
C	8950.958	1	8950.958	8.233	0.0117	
D	5858.438	1	5858.438	5.388	0.0348	
AB	13,925.770	1	13,925.770	12.808	0.0027	
AC	12,085.155	1	12,085.155	11.115	0.0045	
AD	110.093	1	110.093	0.101	0.7547	
BC	12,973.780	1	12,973.780	11.933	0.0035	
BD	9038.780	1	9038.780	8.313	0.0114	
CD	1187.319	1	1187.319	1.092	0.3126	
A^2	254,998.944	1	254,998.944	234.536	<0.0001	
B^2	273,936.683	1	273,936.683	251.954	<0.0001	
C^2	101,752.766	1	101,752.766	93.587	<0.0001	
D^2	112,945.434	1	112,945.434	103.882	<0.0001	
Residuals	16,308.750	15	1087.250			
Lack of fit	14,409.150	10	1440.915	3.793	0.0771	Not significant

Table 4. ANOVA for yield of SBAC.

Source	Sum of Squares	df	Mean Square	F-Value	*p*-Value	
Model	799.940	14	57.139	53.829	<0.0001	Significant
A	126.776	1	126.776	119.432	<0.0001	
B	9.102	1	9.102	8.575	0.0104	
C	10.720	1	10.720	10.099	0.0062	
D	35.235	1	35.235	33.194	<0.0001	
AB	27.826	1	27.826	26.214	0.0001	
AC	10.563	1	10.563	9.951	0.0065	
AD	0.042	1	0.042	0.040	0.8450	
BC	7.563	1	7.563	7.124	0.0175	
BD	13.432	1	13.432	12.654	0.0029	
CD	12.320	1	12.320	11.606	0.0039	
A^2	184.972	1	184.972	174.256	<0.0001	
B^2	297.002	1	297.002	279.797	<0.0001	
C^2	168.102	1	168.102	158.364	<0.0001	
D^2	116.043	1	116.043	109.321	<0.0001	
Residuals	15.922	15	1.061			
Lack of fit	12.077	10	1.208	1.570	0.3229	Not significant

The model exhibits a notable F-value of 48.371, and the associated *p*-value is <0.0001, indicating that the model is significant (Table 3). Within the 95% confidence interval, factors with P-values less than 0.05 are deemed significant [45]. Within the spectrum of process variables, MP emerged as the paramount parameter, boasting an impressive F-value of 89.229 and a *p*-value < 0.001, closely pursued by the impregnation ratio (F-value of 35.125 and a *p*-value < 0.0001). The *p*-values of A^2, B^2, C^2, and D^2 exerted substantial influence on the iodine number.

As depicted in Table 4, the model boasts an F-value of 53.829, aligned with a *p*-value of <0.0001, affirming the model's profound significance. Within the realm of process variables,

IR emerged as the foremost parameter, commanding an impressive F-value of 119.432 and a *p*-value < 0.0001. The *p*-values of A^2, B^2, C^2, and D^2 exerted a noteworthy impact on the yield.

$$Y_1 = 915.38 + 39.89A + 63.58B - 19.31C + 15.63D + 29.5AB - 27.48AC - 2.62AD + 28.47BC - 23.77BD + 8.61CD - 96.42A^2 - 99.94B^2 - 60.9C^2 - 64.17D^2 \quad (3)$$

$$Y_2 = 47.328 + 2.298A + 0.615B + 0.668C + 1.21D + 1.32AB - 0.8125AC + 0.05AD - 0.6875BC + 0.8775CD - 2.597A^2 - 3.29B^2 - 2.476C^2 - 2.057D^2 \quad (4)$$

The complex correlation coefficient (R^2) of the model characterizes the correlation of each model, and the larger its value, the better the fitting effect of the model; the difference between the correction coefficient of determination (R^2_{adj}) and the prediction coefficient of determination (R^2_{pred}) is less than 0.2, and the larger the value of the two coefficients, the better the interpretation of the model. The index used to reflect the degree of model variation is the coefficient of variation (C.V.), and when it is less than 10%, it indicates that the test results are reliable [46].

In this study, the fitting accuracies of SBAC, the obtained R^2 and R^2_{adj} are both >0.9 and tend to be close to 1, indicating that the model can accurately describe the experimental results (Table 5). The difference between R^2_{adj} and R^2_{pred} of the two models is 0.0723 and 0.0543, respectively, both <0.2, which shows that the fitting accuracy of both models is better and the sampling error is smaller [47]. The C.V. of the models is 5.02% and 2.64%, respectively, both lower than 10%, indicating that the models have good accuracy and reliability and are suitable for experimental analysis.

Residual error analysis can detect the relevance of the model and the reliability of the data, and the residuals should obey a normal distribution without considering the experimental outliers [48]. The standardized residual values of each model have only two test points outside the interval of (−3, 3), which indicates that the distribution of each test point is random and presents irregular characteristics, proving the reasonableness of the test point-taking points (Figure 3). In addition, all test points are uniformly distributed on a straight line, and only a very few are discrete, so the standardized residuals of each model are normally distributed, which can reasonably explain the regression of the model.

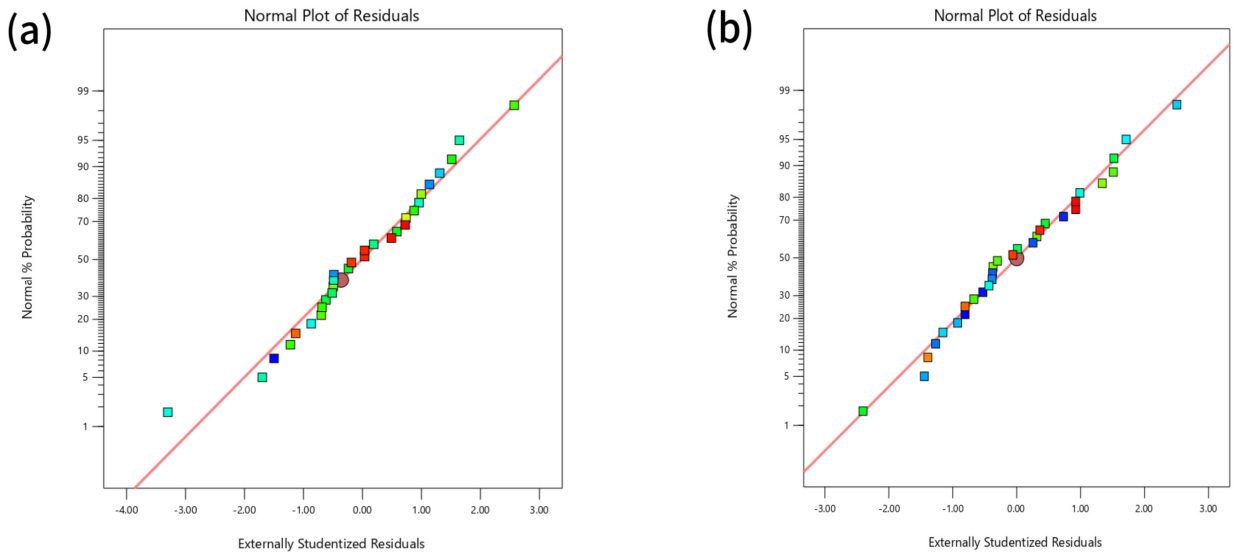

Figure 3. Distribution of residuals for each model: (**a**) iodine number of SBAC; (**b**) SBAC yield.

Table 5. Accuracy of the fit for SBAC.

Model	R^2	R^2_{adj}	R^2_{pred}	C.V./(%)
Iodine number	0.9783	0.9580	0.8857	5.02
Yield	0.9805	0.9623	0.9080	2.64

3.2.3. Response Surface Interaction Analysis

Three-dimensional curves of response surfaces were plotted using Design Expert 13.2 software to explore the interaction of the designated two factors on iodine number and SBAC yield. Figures 4 and 5 illustrate the response surface analysis of the joint effects of IR, MP, microwave irradiation time, and biomass bed depth on iodine number and yield, respectively. The interacting contours of these interactions are elliptical, indicating a significant interaction of the two factors in the figure. The interaction of IR and power on iodine number is shown in Figure 4a, and the biomass bed depth and microwave irradiation duration at the level of 0 are shown in Figure 4a. In the experimental scope, the SBAC iodine number increases and then decreases with the increase in the IR; similarly, at a constant IR, with an increase in the power, the SBAC iodine number also increased first and then decreased. Figure 4c shows the interaction effect of time and IR on the adsorption value of SBAC iodine, and its rule of change is similar to that of Figure 4a, but the magnitude of the change is smaller, which indicates that the interaction between IR and power is larger than the interaction between IR and time. While observing Figure 4b, it can be seen that when the height of the biomass bed is at the same level, the iodine number of SBAC almost shows an upward trend with the increase in IR, and slowly decreases when the IR reaches about 2.3, and at this time, it can reach the center of the interaction effect, i.e., at this time, the interaction effect of the height of the biomass bed and the IR on the iodine number of SBAC is the most obvious.

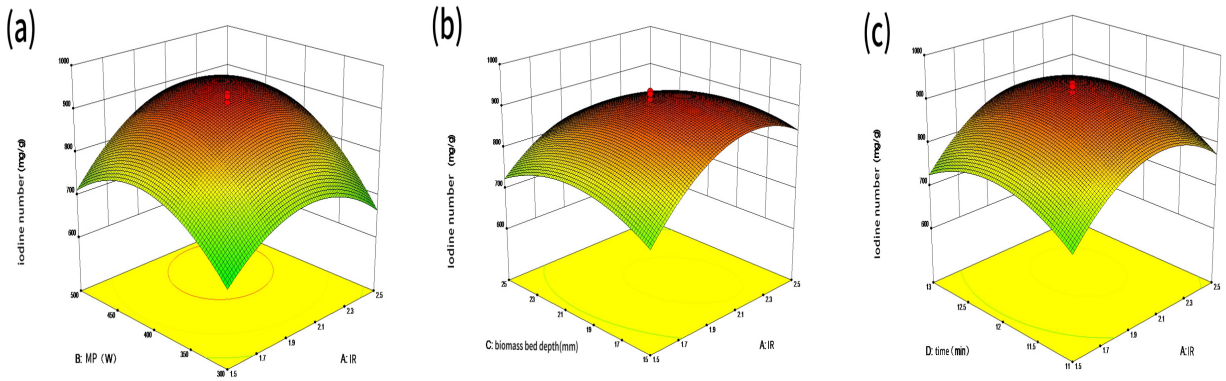

Figure 4. Combined effects of (**a**) IR and MP, (**b**) IR and biomass bed depth, and (**c**) IR and time on iodine number of SBAC.

A parallel pattern is evident in Figure 5; each factor exhibits an optimum value within the experimental range. When one factor is held constant, the other factor can still identify the pinnacle point within the experimental range. However, their combined influence is diminished, as the curves exhibit minimal variability.

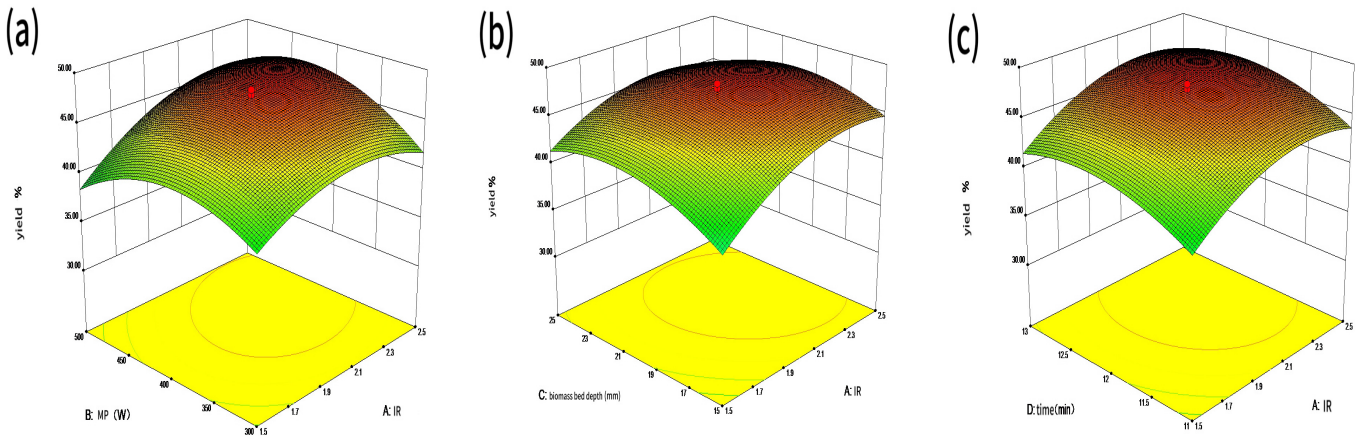

Figure 5. Combined effects of (**a**) IR and MP, (**b**) IR and biomass bed depth, and (**c**) IR on the yield of SBAC.

3.2.4. Model Validation and Optimal Process Conditions

The optimal values (yield and iodine number) for the SBAC were derived through various process parameters. In this investigation, Design Expert 13.2 software facilitated the numerical optimization of the two response factors, with the optimized process slope shape shown in Figure 6. The optimal conditions for achieving the maximum iodine number and yield of SBAC were determined as follows: IR of 2.47, MP of 479.07 W, biomass bed depth of 23.86 mm, and an irradiation time of 12.96 min. The numerically optimized values from the RSM for the maximum SBAC iodine number and yield are succinctly compiled in Table 6. Under these optimal conditions, the predicted iodine number reached 868.70 mg/g, and the yield stood at 43.88%. The validity of the predicted values in the optimization test was verified experimentally. The experimental results showed that the iodine number was 918.30 mg/g and the yield was 43.02%, and these measurements were in good agreement with the predicted values, and the differences in SBAC iodine number and yield were 5.40% and 1.90%, respectively; these slight deviations (within 10%) between the predicted and experimental values show the accuracy of the optimization process.

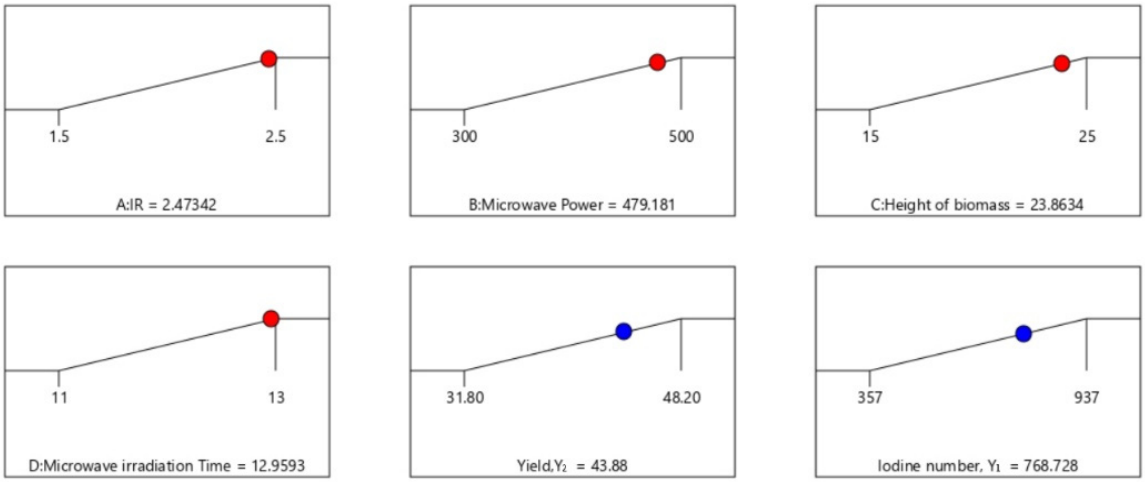

Figure 6. Optimized process slope shape.

Table 6. Comparison of experimental and model-predicted values of SBAC performance.

Satisfaction	Impact Factor				Iodine Number/(mg/g)		Iodine Number Error/%	Yield/%		Yield Error/%
	A	*B*	*C*	*D*	Experimental Value	Predicted Value		Experimental Value	Predicted Value	
0.86	2.47	479.07	23.86	12.96	918.3	868.70	5.4	43.02	43.88	1.9

3.3. Characteristic Features of SB and SBAC Produced under Optimal Conditions

3.3.1. Fourier Transform Infrared (FTIR) Analysis

Figure 7a,b show the infrared spectra of two materials, SB and SBAC, and Figure 7b presents the enlarged 2000–1200 cm^{-1} region of the spectra. SB is a typical biomass containing cellulose, hemicellulose, and lignin. From their FTIR diagrams, it can be seen that the absorption peak near 3431 cm^{-1} can be attributed to the O-H stretching vibration peaks of polysaccharides and water in SB; the absorption peak located near 2902 cm^{-1} is the aliphatic C-H stretching vibration peak; the absorption peak near 1635 cm^{-1} is attributed to the C=C stretching vibrational peak in lignin; the absorption peak near 1572 cm^{-1} is mainly attributed to the O-H bending vibrational peak in xyloglucan-type polysaccharides absorbing water; the absorption peak near 1416 cm^{-1} is a bending vibrational peak in cellulose -CH_2; The absorption peak near 1131 cm^{-1} is related to the asymmetric deformation of C-O-C in cellulose and hemicellulose; the absorption peak near 1051 cm^{-1} can be attributed to the C-O stretching vibration peak in cellulose; the absorption peak near 644 cm^{-1} can be attributed to the bending vibration peak of aromatic compounds [49]. From the FTIR spectrum of the pyrolyzed SBAC material, it can be seen that the absorption peak located near 2902 cm^{-1} is weakened, which may be due to the breakage of the weak bond between alkyl C-H due to pyrolysis. Meanwhile, no absorption peak of C=O was observed near 1741 cm^{-1}, which indicates that the material undergoes a decarbonylation reaction after pyrolysis to produce CO_2. It can be seen from the figure that the aromatic structure of the AC material after pyrolysis is stronger, the polarity is reduced, and the adsorption capacity is enhanced.

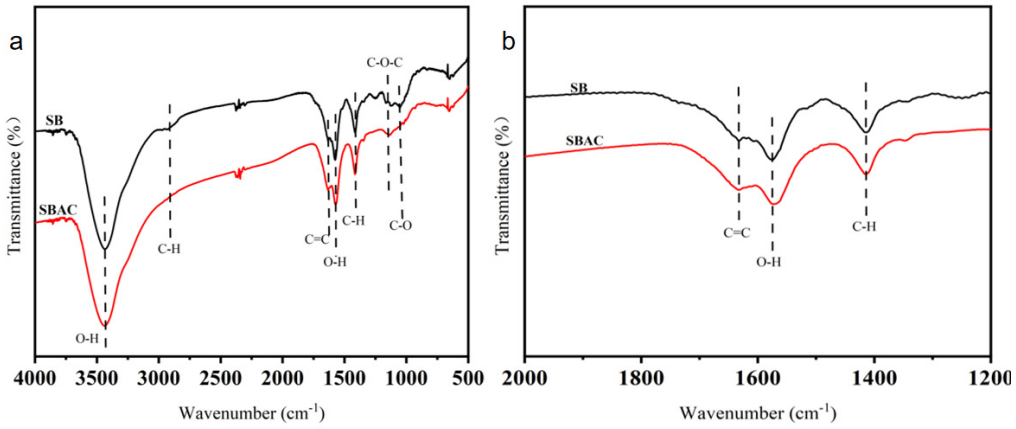

Figure 7. (**a**,**b**). FTIR of SB and SBAC.

3.3.2. Brunauer–Emmett–Teller (BET) Analysis

The N_2 adsorption–desorption isotherms and pore size distribution of SBAC are shown in Figure 8. According to the IUPAC classification, they exhibit intermediate characteristics between type II and type IV. The stage at the low-pressure end near the *Y*-axis is dominated by micropores exerting adsorption. A hysteresis loop appears in the medium-pressure stage, which proves that the AC is a graded porous carbon material with predominantly micropores, mesopores, and macropores. The textural characteristics were obtained using the t-plot method, and pore size distribution was determined using the BJH model. The porosity of this SBAC contains both micropores and mesopores. The average pore diameter

of 7.50 nm confirms the presence of this mesoporosity. The specific surface area and total pore volume of SBAC products are listed in Table 7.

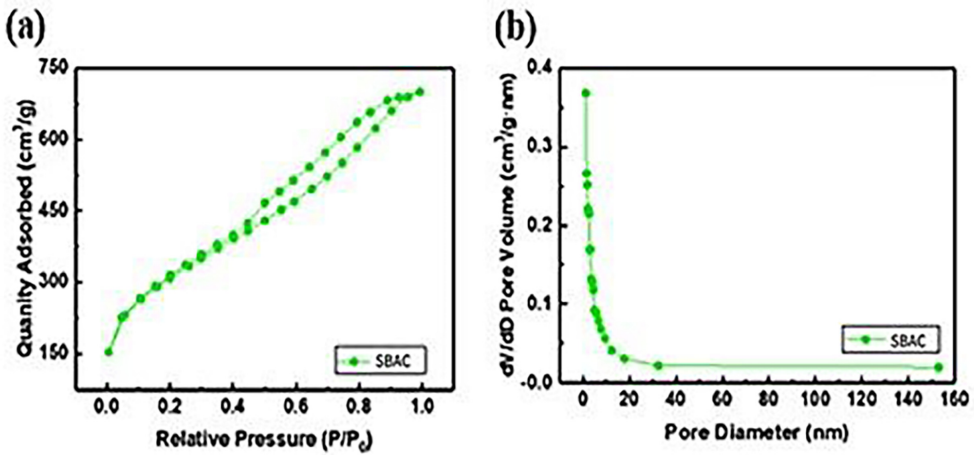

Figure 8. SBAC N_2 adsorption–desorption isotherms (**a**) and pore size distribution (**b**).

Table 7. Product parameters of SBAC.

Materials	Specific Surface Area (m^2/g)	Total Hole Volume (cm^3/g)
Sugarcane bagasse carbon	1697.367	1.202

Congsomjit [50] has reported SBAC using hydrothermal carbonization with a maximum specific surface area of 390 m^2/g, far less than the sample in this study. The maximum specific surface area of SBAC under optimal conditions produced was 1697.367 m^2/g, which is greater than commercial activated carbons (500–1500 m^2/g). Therefore, microwave pyrolysis shows great potential for the production of activated carbon.

3.3.3. SEM Analysis

Figure 9 shows the morphological characterization of the bagasse feedstock. It can be seen that the bagasse feedstock is a mostly rod-like structure, with a few flakes accompanied by an obvious linear structure.

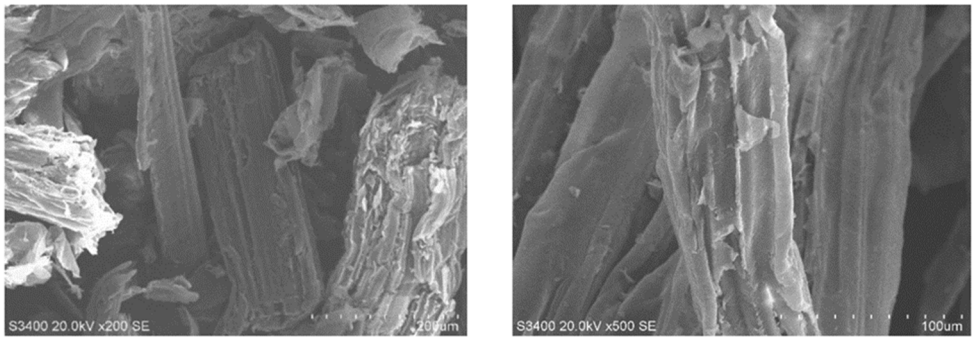

Figure 9. SEM image of SB.

After activation and pyrolysis, the shape of SB changes considerably (Figure 10). The richer and more developed honeycomb pore structure increases the specific surface area of the SBAC, and the larger pore structure has the property of easy adsorption of macromolecules of organic matter, which is suitable for application in the treatment of water pollution as well as the storage of energy. During the activation process, carbon reacts with steam to produce a large number of mesopores, which greatly increases the surface

area of SBAC. Compared with the raw material of SB, which has no pores and a rough surface, it can be concluded that MVP formed a highly porous structure inside SBAC.

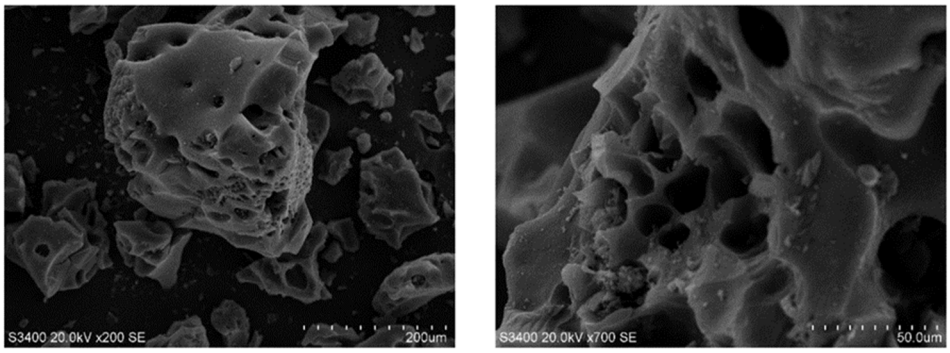

Figure 10. SEM diagram of the SBAC.

4. Conclusions

The synthesis of SBAC through microwave pyrolysis in this investigation introduces a cost-effective and eco-friendly methodology for efficient management and valorization of agricultural waste. The impacts of IR, MP, biomass bed depth, and microwave irradiation time on SBAC iodine number and yield were systematically explored. The optimized parameters determined were 479.07 W, 12.96 min, 23.86 mm, and 2.47 IR, yielding responses of 43.88% and 868.70 mg/g for yield and iodine number, respectively. The model-predicted outcomes were substantiated, revealing a marginal 5.4% variance in yield and a mere 1.9% discrepancy in iodine number from the anticipated values. The morphological and chemical attributes of the synthesized SBAC, evaluated through FTIR, BET, and SEM, underscore its potential as a versatile adsorbent. The utilization of cost-effective SBAC as an adsorbent holds promise for both economic and environmental advantages by repurposing waste bagasse.

Author Contributions: Methodology, X.W.; data curation, Y.P.; writing—original draft preparation, X.C.; writing—review and editing, L.J.; funding acquisition, W.Z. All authors have read and agreed to the published version of the manuscript.

Funding: The authors acknowledge the support of grants from the education department of National Natural Science Foundation of China (41907116), Basic Research Program of Jiangsu Province (BK20191040), Changzhou Science and Technology Program (International Science and Technology Cooperation) Project (CZ20170020), and Jiangsu Graduate Practice Innovation Program (XSJCX22_77).

Data Availability Statement: Data are contained within the article.

Conflicts of Interest: The authors declare no conflicts of interest.

References

1. Souza, M.A.D.; Vilas-Boas, I.T.; Leite-da-Silva, J.M.; Abrahão, P.D.N.; Teixeira-Costa, B.E.; Veiga-Junior, V.F. Polysaccharides in Agro-Industrial Biomass Residues. *Polysaccharides* **2022**, *3*, 95–120. [CrossRef]
2. He, K.; Zhang, J.; Zeng, Y. Knowledge Domain and Emerging Trends of Agricultural Waste Management in the Field of Social Science: A Scientometric Review. *Sci. Total Environ.* **2019**, *670*, 236–244. [CrossRef]
3. Mujahid, R.; Riaz, A.; Insyani, R.; Kim, J. A Centrifugation-First Approach for Recovering High-Yield Bio-Oil with High Calorific Values in Biomass Liquefaction: A Case Study of Sewage Sludge. *Fuel* **2020**, *262*, 116628. [CrossRef]
4. Quillope, J.C.C.; Carpio, R.B.; Gatdula, K.M.; Detras, M.C.M.; Doliente, S.S. Optimization of Process Parameters of Self-Purging Microwave Pyrolysis of Corn Cob for Biochar Production. *Heliyon* **2021**, *7*, e08417. [CrossRef]
5. Xu, Q.; Ji, T.; Gao, S.-J.; Yang, Z.; Wu, N. Characteristics and Applications of Sugar Cane Bagasse Ash Waste in Cementitious Materials. *Materials* **2018**, *12*, 39. [CrossRef]
6. Inácio, J.G.; Ferreira, M.D.A.; Silva, R.C.; Silva, J.D.L.; Oliveira, J.C.V.D.; Santos, D.C.D.; Soares, L.F.P.; Campos, J.M.D.S. Sugarcane Bagasse as Exclusive Roughage for Dairy Heifers. *Rev. Bras. Zootec.* **2017**, *46*, 80–84. [CrossRef]

7. Brunerová, A.; Roubík, H.; Brožek, M.; Van Dung, D.; Phung, L.D.; Hasanudin, U.; Iryani, D.A.; Herák, D. Briquetting of Sugarcane Bagasse as a Proper Waste Management Technology in Vietnam. *Waste Manag. Res.* **2020**, *38*, 1239–1250. [CrossRef] [PubMed]
8. Iwuozor, K.O.; Oyekunle, I.P.; Oladunjoye, I.O.; Ibitogbe, E.M.; Olorunfemi, T.S. A Review on the Mitigation of Heavy Metals from Aqueous Solution Using Sugarcane Bagasse. *Sugar Tech* **2022**, *24*, 1167–1185. [CrossRef]
9. Liu, Y.; Zheng, X.; Tao, S.; Hu, L.; Zhang, X.; Lin, X. Process Optimization for Deep Eutectic Solvent Pretreatment and Enzymatic Hydrolysis of Sugar Cane Bagasse for Cellulosic Ethanol Fermentation. *Renew. Energy* **2021**, *177*, 259–267. [CrossRef]
10. Wang, Q.; Wang, W.; Tan, X.; Zahoor; Chen, X.; Guo, Y.; Yu, Q.; Yuan, Z.; Zhuang, X. Low-Temperature Sodium Hydroxide Pretreatment for Ethanol Production from Sugarcane Bagasse without Washing Process. *Bioresour. Technol.* **2019**, *291*, 121844. [CrossRef] [PubMed]
11. Dionísio, S.R.; Santoro, D.C.J.; Bonan, C.I.D.G.; Soares, L.B.; Biazi, L.E.; Rabelo, S.C.; Ienczak, J.L. Second-Generation Ethanol Process for Integral Use of Hemicellulosic and Cellulosic Hydrolysates from Diluted Sulfuric Acid Pretreatment of Sugarcane Bagasse. *Fuel* **2021**, *304*, 121290. [CrossRef]
12. Gautam, P.; Neha; Upadhyay, S.N.; Dubey, S.K. Bio-Methanol as a Renewable Fuel from Waste Biomass: Current Trends and Future Perspective. *Fuel* **2020**, *273*, 117783. [CrossRef]
13. Shahbaz, M.; AlNouss, A.; Ghiat, I.; Mckay, G.; Mackey, H.; Elkhalifa, S.; Al-Ansari, T. A Comprehensive Review of Biomass Based Thermochemical Conversion Technologies Integrated with CO_2 Capture and Utilisation within BECCS Networks. *Resour. Conserv. Recycl.* **2021**, *173*, 105734. [CrossRef]
14. Kwon, E.E.; Kim, S.; Lee, J. Pyrolysis of Waste Feedstocks in CO_2 for Effective Energy Recovery and Waste Treatment. *J. CO2 Util.* **2019**, *31*, 173–180. [CrossRef]
15. Allende, S.; Brodie, G.; Jacob, M.V. Energy Recovery from Sugarcane Bagasse under Varying Microwave-Assisted Pyrolysis Conditions. *Bioresour. Technol. Rep.* **2022**, *20*, 101283. [CrossRef]
16. Selvam, S.M.; Paramasivan, B. Microwave Assisted Carbonization and Activation of Biochar for Energy-Environment Nexus: A Review. *Chemosphere* **2022**, *286*, 131631. [CrossRef] [PubMed]
17. Shukla, N.; Sahoo, D.; Remya, N. Biochar from Microwave Pyrolysis of Rice Husk for Tertiary Wastewater Treatment and Soil Nourishment. *J. Clean. Prod.* **2019**, *235*, 1073–1079. [CrossRef]
18. Lee, X.J.; Ong, H.C.; Gan, Y.Y.; Chen, W.-H.; Mahlia, T.M.I. State of Art Review on Conventional and Advanced Pyrolysis of Macroalgae and Microalgae for Biochar, Bio-Oil and Bio-Syngas Production. *Energy Convers. Manag.* **2020**, *210*, 112707. [CrossRef]
19. Putra, P.H.M.; Rozali, S.; Patah, M.F.A.; Idris, A. A Review of Microwave Pyrolysis as a Sustainable Plastic Waste Management Technique. *J. Environ. Manag.* **2022**, *303*, 114240. [CrossRef] [PubMed]
20. Lam, S.S.; Wan Mahari, W.A.; Ma, N.L.; Azwar, E.; Kwon, E.E.; Peng, W.; Chong, C.T.; Liu, Z.; Park, Y.-K. Microwave Pyrolysis Valorization of Used Baby Diaper. *Chemosphere* **2019**, *230*, 294–302. [CrossRef]
21. Robinson, J.; Binner, E.; Vallejo, D.B.; Perez, N.D.; Al Mughairi, K.; Ryan, J.; Shepherd, B.; Adam, M.; Budarin, V.; Fan, J.; et al. Unravelling the Mechanisms of Microwave Pyrolysis of Biomass. *Chem. Eng. J.* **2022**, *430*, 132975. [CrossRef]
22. Xu, D.; Lin, J.; Sun, S.; Ma, R.; Wang, M.; Yang, J.; Luo, J. Microwave Pyrolysis of Biomass Model Compounds for Bio-Oil: Formation Mechanisms of the Nitrogenous Chemicals and DFT Calculations. *Energy Convers. Manag.* **2022**, *262*, 115676. [CrossRef]
23. He, X.; Chen, X.; Wang, X.; Jiang, L. Optimization of Activated Carbon Production from Corn Cob Using Response Surface Methodology. *Front. Environ. Sci.* **2023**, *11*, 1105408. [CrossRef]
24. Parvez, A.M.; Wu, T.; Afzal, M.T.; Mareta, S.; He, T.; Zhai, M. Conventional and Microwave-Assisted Pyrolysis of Gumwood: A Comparison Study Using Thermodynamic Evaluation and Hydrogen Production. *Fuel Process. Technol.* **2019**, *184*, 1–11. [CrossRef]
25. Wallace, C.A.; Afzal, M.T.; Saha, G.C. Effect of Feedstock and Microwave Pyrolysis Temperature on Physio-Chemical and Nano-Scale Mechanical Properties of Biochar. *Bioresour. Bioprocess.* **2019**, *6*, 33. [CrossRef]
26. Cheng, S.; Meng, M.; Xing, B.; Shi, C.; Nie, Y.; Xia, D.; Yi, G.; Zhang, C.; Xia, H. Preparation of Valuable Pyrolysis Products from Poplar Waste under Different Temperatures by Pyrolysis: Evaluation of Pyrolysis Products. *Bioresour. Technol.* **2022**, *364*, 128011. [CrossRef] [PubMed]
27. Shi, K.; Yan, J.; Menéndez, J.A.; Luo, X.; Yang, G.; Chen, Y.; Lester, E.; Wu, T. Production of H2-Rich Syngas From Lignocellulosic Biomass Using Microwave-Assisted Pyrolysis Coupled With Activated Carbon Enabled Reforming. *Front. Chem.* **2020**, *8*, 3. [CrossRef] [PubMed]
28. Liew, R.K.; Chong, M.Y.; Osazuwa, O.U.; Nam, W.L.; Phang, X.Y.; Su, M.H.; Cheng, C.K.; Chong, C.T.; Lam, S.S. Production of Activated Carbon as Catalyst Support by Microwave Pyrolysis of Palm Kernel Shell: A Comparative Study of Chemical versus Physical Activation. *Res Chem Intermed* **2018**, *44*, 3849–3865. [CrossRef]
29. Rodier, L.; Bilba, K.; Onésippe, C.; Arsène, M.-A. Utilization of Bio-Chars from Sugarcane Bagasse Pyrolysis in Cement-Based Composites. *Ind. Crops Prod.* **2019**, *141*, 111731. [CrossRef]
30. Guo, Y.; Tan, C.; Sun, J.; Li, W.; Zhang, J.; Zhao, C. Porous Activated Carbons Derived from Waste Sugarcane Bagasse for CO_2 Adsorption. *Chem. Eng. J.* **2020**, *381*, 122736. [CrossRef]
31. Torgbo, S.; Quan, V.M.; Sukyai, P. Cellulosic Value-Added Products from Sugarcane Bagasse. *Cellulose* **2021**, *28*, 5219–5240. [CrossRef]
32. Siddique, I.J.; Salema, A.A.; Antunes, E.; Vinu, R. Technical Challenges in Scaling up the Microwave Technology for Biomass Processing. *Renew. Sustain. Energy Rev.* **2022**, *153*, 111767. [CrossRef]

33. Smucker, B.; Krzywinski, M.; Altman, N. Optimal Experimental Design. *Nat. Methods* **2018**, *15*, 559–560. [CrossRef]
34. Yolmeh, M.; Jafari, S.M. Applications of Response Surface Methodology in the Food Industry Processes. *Food Bioprocess Technol.* **2017**, *10*, 413–433. [CrossRef]
35. Sahu, P.K.; Ramisetti, N.R.; Cecchi, T.; Swain, S.; Patro, C.S.; Panda, J. An Overview of Experimental Designs in HPLC Method Development and Validation. *J. Pharm. Biomed. Anal.* **2018**, *147*, 590–611. [CrossRef]
36. Khan, O.; Khan, M.Z.; Bhatt, B.K.; Alam, M.T.; Tripathi, M. Multi-Objective Optimization of Diesel Engine Performance, Vibration and Emission Parameters Employing Blends of Biodiesel, Hydrogen and Cerium Oxide Nanoparticles with the Aid of Response Surface Methodology Approach. *Int. J. Hydrogen Energy* **2023**, *48*, 21513–21529. [CrossRef]
37. Hou, F.; Mu, T.; Ma, M.; Blecker, C. Optimization of Processing Technology Using Response Surface Methodology and Physicochemical Properties of Roasted Sweet Potato. *Food Chem.* **2019**, *278*, 136–143. [CrossRef]
38. Peng, Y.D.; Zhang, Z.J.; Wang, X.Q.; Liu, S.D.; Yang, A.H.; Wang, X.S. Frequency and Intensity Readouts of Micro-Wave Electric Field Using Rydberg Atoms with Doppler Effects. *Opt. Quantum Electron.* **2018**, *50*, 311. [CrossRef]
39. Brazil, T.R.; Gonçalves, M.; Junior, M.S.O.; Rezende, M.C. A Statistical Approach to Optimize the Activated Carbon Production from Kraft Lignin Based on Conventional and Microwave Processes. *Microporous Mesoporous Mater.* **2020**, *308*, 110485. [CrossRef]
40. Yan, Q.; Li, J.; Cai, Z. Preparation and Characterization of Chars and Activated Carbons from Wood Wastes. *Carbon Lett.* **2021**, *31*, 941–956. [CrossRef]
41. Kurgankina, M.; Nyashina, G.; Shvets, A.; Vershinina, K.; Pereira Junior, A.O. Microwave Pyrolysis of Biomass: The Influence of Surface Area and Structure of a Layer. *Appl. Sci.* **2022**, *12*, 12442. [CrossRef]
42. Heidarinejad, Z.; Dehghani, M.H.; Heidari, M.; Javedan, G.; Ali, I.; Sillanpää, M. Methods for Preparation and Activation of Activated Carbon: A Review. *Environ. Chem. Lett* **2020**, *18*, 393–415. [CrossRef]
43. Yek, P.N.Y.; Liew, R.K.; Osman, M.S.; Lee, C.L.; Chuah, J.H.; Park, Y.-K.; Lam, S.S. Microwave Steam Activation, an Innovative Pyrolysis Approach to Convert Waste Palm Shell into Highly Microporous Activated Carbon. *J. Environ. Manag.* **2019**, *236*, 245–253. [CrossRef]
44. Barreno-Avila, E.; Moya-Moya, E.; Pérez-Salinas, C. Rice-Husk Fiber Reinforced Composite (RFRC) Drilling Parameters Optimization Using RSM Based Desirability Function Approach. *Mater. Today Proc.* **2022**, *49*, 167–174. [CrossRef]
45. Das, S.; Goud, V.V. RSM-Optimised Slow Pyrolysis of Rice Husk for Bio-Oil Production and Its Upgradation. *Energy* **2021**, *225*, 120161. [CrossRef]
46. Kumari, M.; Gupta, S.K. Response Surface Methodological (RSM) Approach for Optimizing the Removal of Trihalomethanes (THMs) and Its Precursor's by Surfactant Modified Magnetic Nanoadsorbents (sMNP)—An Endeavor to Diminish Probable Cancer Risk. *Sci. Rep.* **2019**, *9*, 18339. [CrossRef]
47. Beyan, S.M.; Prabhu, S.V.; Sissay, T.T.; Getahun, A.A. Sugarcane Bagasse Based Activated Carbon Preparation and Its Adsorption Efficacy on Removal of BOD and COD from Textile Effluents: RSM Based Modeling, Optimization and Kinetic Aspects. *Bioresour. Technol. Rep.* **2021**, *14*, 100664. [CrossRef]
48. Park, K.; Jung, D.; Kim, J.-M. Control Charts Based on Randomized Quantile Residuals. *Appl. Stoch. Models Bus. Ind.* **2020**, *36*, 716–729. [CrossRef]
49. Yadav, M.S.; Singh, N.; Bobade, S.M. VxOy Nanoparticles and Activated Charcoal Based Nanocomposite for Supercapacitor Electrode Application. *Ionics* **2020**, *26*, 2581–2598. [CrossRef]
50. Congsomjit, D.; Areeprasert, C. Hydrochar-Derived Activated Carbon from Sugar Cane Bagasse Employing Hydrothermal Carbonization and Steam Activation for Syrup Decolorization. *Biomass Convers. Biorefinery* **2021**, *11*, 2569–2584. [CrossRef]